Research

Removal of rhodamine B and methylene blue using residual *Onecarpus bacaba* Mart fibers as biosorbent: kinetic and thermodynamic parameters

Eberlanny Moraes Rolim[1] · Andreza Miranda Barata da Silva[1] · Joel dos Santos Batista[1] ·
Naiany Oliveira Serrão[1] · Leticia Oliveira Laier[2] · Flávio Augusto de Freitas[3] · Gustavo Frigi Perotti[1] ·
Dominique Fernandes de Moura do Carmo[1] · Gustavo de Gusmão Celestino[4] · Paulo José Sousa Maia[2]

Abstract
Among the most common water contaminants, dyes are responsible for polluting rivers and other water bodies as well as contributing to other environmental problems, thus posing serious health hazards to humans and animals. In order to minimize these environmental impacts, this study proposes the use of *Onecarpus bacaba* Mart fiber residues, *in natura* (OBMi) and NaOH-modified (OBMm), to bioadsorb rhodamine b (RhB) and methylene blue (MB) dyes. The biosorbents OBMi and OBMm were characterized by means of infrared spectroscopy, thermogravimetric analysis, X-ray diffraction, Boehm titration, PZC, and scanning electron microscopy. This study also analyzed the influence of pH, contact time, absorbent mass, temperature, and contaminant concentrations by means of batch equilibrium assays. It was observed that the OBMi absorbent showed a low dye removal capacity. Maximum OBMm adsorption capacity for RhB and MB at 25 °C was 26.60 mg g^{-1} and 407.98 mg g^{-1}, respectively. In both systems, OBMm:RhB and OBMm:MB, adsorption kinetics followed a pseudo-second-order model, and the Langmuir and Freundlich models constituted the best fit for isothermal curves. Lastly, thermodynamic parameters indicated that adsorption of both RhB and MB onto OBMm is spontaneous.

Keywords Adsorption · *Onecarpus bacaba* · Dye removal · Wastewater

---

✉ Paulo José Sousa Maia, pmldcb@gmail.com; Eberlanny Moraes Rolim, eberlanny@gmail.com; Andreza Miranda Barata da Silva, andrezamirandab@gmail.com; Joel dos Santos Batista, santosjoel229@gmail.com; Naiany Oliveira Serrão, naiany.band@gmail.com; Leticia Oliveira Laier, leticialol@hotmail.com; Flávio Augusto de Freitas, Freitas.flavio@yahoo.com.br; Gustavo Frigi Perotti, gustavofrigi@gmail.com; Dominique Fernandes de Moura do Carmo, dominiquefmc@ufam.edu.br; Gustavo de Gusmão Celestino, gusmao11@gmail.com | [1]Instituto de Ciências Exatas e Tecnologia, Universidade Federal do Amazonas, Itacoatiara, Amazonas 69103128, Brasil. [2]Grupo de Eletrocatálise e Química Bioinorgânica (GEQBio), Universidade Federal do Rio de Janeiro, 27930-560 Macaé, Rio de Janeiro, Brasil. [3]Centro de Biotecnologia da Amazônia-CBA, Av. Gov. Danilo de Matos Areosa, 690-Distrito Industrial I, Manaus, AM 69075-351, Brasil. [4]Programa de Engenharia Metalúrgica e de Materiais/COPPE/LADPOL, Universidade Federal do Rio de Janeiro, Av. Horácio Macedo, 2030, Bloco F, 21941598 Rio de Janeiro, RJ, Brasil.

1 Introduction

Global concerns about fresh water go beyond its pending scarcity; they also include the impact on ecosystems caused by industrial discharges of contaminants, such as heavy metals, dyes, drugs, and pesticides, into rivers, lakes, and other water bodies [1–3]. Several sustainability programs and initiatives have been proposed in response to this important environmental and social challenge [4]. The most recent initiative is the 2030 Agenda, whose objectives comprise outlining strategies for improving the quality of freshwater by reducing pollution caused by toxic chemicals released into water bodies [5].

Widely used in industry, dyes can cause serious pollution problems when inadequately discharged into water bodies. Accumulation of dyes in nature negatively affects ecological balance and human health, since most of them are toxic, carcinogenic, and non-biodegradable [6].

Among the most common dyes are rhodamine B (RhB) and methylene blue (MB). A cationic dye, RhB has been identified as a Grade 3 carcinogen by the International Agency for Research on Cancer (IARC) due to its toxicity and potential carcinogenic mutagenicity [7–9]. On the other hand, despite not exhibiting high toxicity and even being occasionally used as medicine, the presence of MB in water can still have harmful effects on living organisms as it does not degrade easily [10, 11]. Extended exposure to MB has been known to cause eye irritation, tachycardia, vomiting, and delayed mental maturation.

Several processes are presently employed for removing pollutants from effluents, such as ion exchange, electrokinetic coagulation, membrane filtration, and adsorption. Among these processes, adsorption has been widely used due to its low cost, thermal and chemical stability, selectivity, and high removal capacity for different types of dyes [3, 12].

In adsorption processes, activated carbon is the most frequently used adsorbent, owing to its large specific area, micro-pore characteristics, and high adsorption capacity [13]. Notwithstanding these advantages, the use of activated carbon is costly in large-scale operations as it needs to be regenerated after every adsorption cycle [13]. For this reason, lignocellulosic materials, such as biosorbents, have been proposed as alternatives.

Several researchers have investigated the use of agro-industrial residues as biosorbents to remove contaminants from water bodies. Some biomasses have shown satisfactory results in RhB and MB absorption, such as coconut waste [8], rice straws [10], almond husks [14], rosemary residues [9], walnut shells [2, 15], banana peels [16], *Rhus coriaria* L. (*Anacardiaceae*) [17], *Clitoria fairchildiana* [18], and black tea residues [7].

In this vein, this study was carried out with fiber residues from production of abacaba trees (*Oenocarpus bacaba* Mart) (OBM), a fruit species native to the Amazon region. Found throughout the Amazon Basin, with higher frequency in the states of Amazonas and Pará, Brazil, the habitat of OBM consists of pristine high-altitude *terra-firme* forests [19]. OBM is a thornless palm tree, with a sole, smooth, straight trunk up to 20 m high. This palm tree belongs to the *Arecaceae* family, the third most economically important botanical family after the *Poaceae* and *Fabaceae* families. The *Arecaceae* family comprises over 2500 species distributed into 200 genera occurring mostly in the tropics [19].

The sustainability of OBM farming in the Amazonic region can vary depending on local practices and management. In some areas, sustainable farming practices are employed, while in others, there may be issues related to deforestation and unsustainable land use. Ex situ conservation, one of the most common approaches, has demonstrated its superiority over other conservation methods. Embrapa Amazônia Oriental has notably established and currently manages the sole Active Germplasm Bank for Oenocarpus, known as the Bacabas Germplasm Bank (BAG) [20]. This BAG, initiated in 1989, is located at the institution's headquarters in Belém, PA, and consists of field cultivation with plants spaced at 7×7 m intervals. Within this setting, BAG accessions undergo characterization and evaluation for fruit production characteristics and processed pulp quality. Nevertheless, this conservation approach, despite its expansive land requirements and associated costs, falls short of ensuring the long-term preservation of the natural variability.

Given the above, this study presents the removal of RhB and MB dyes (Fig. 1) from synthetic solutions using *in natura* and modified OBM fibers (OBMi and OBMm, respectively) as biosorbents.

2 Materials and method

2.1 Chemicals

RhB and MB stock solutions (0.01 mol L^{-1}) were prepared weekly with double-distilled water. Then, these stock solutions were diluted with double-distilled water until reaching the adsorbate concentrations required for the assays. In order to quantity the surface functional groups of OBMi and OBMm, NaCl ($\geq$ 98%), NaHCO$_3$ ($\geq$ 99.7%),

Fig. 1 Representation of the structures of the dyes used in this study: (**A**) rhodamine b (RhB) and (**B**) methylene blue (MB)
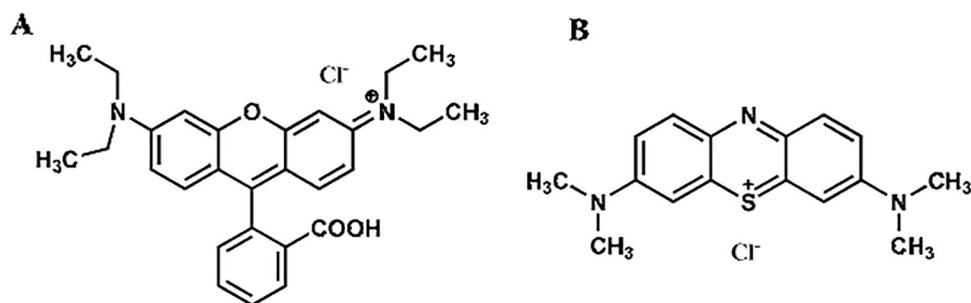
and Na_2CO_3 (≥ 99.0%) were used. For pH adjustment, NaOH (98%) and HCl (37%) solutions were used. All reagents were purchased from Sigma Aldrich.

2.2 *Oenocarpus bacaba* Mart processing

OBM fibers were collected on the ground in rural areas of Itacoatiara (3°08′ 01.65′′ S 58° 26′ 19.04′′ W), Amazonas State, Brazil (Fig. 2a). They were washed, dried for 24 h at 60 °C in an oven with air circulation, manually separated from seeds, and ground in a knife mill (ACB Labor). The resulting material was sieved through a 100 mesh sieve (150 μm) and labeled as OBMi (Fig. 2b).

For the alkaline modification, 10 g of OBM fibers were placed in contact with an aqueous NaOH solution (4.0% w/v). Then, the system was left to rest for 24 h. Next, the fibers were washed with distilled water until the supernatant pH was close to neutral. Subsequently, the NaOH-modified adsorbent was dried in an oven at 60 °C for 24 h and labeled as OBMm (Fig. 2c).

2.3 OBM characterization

2.3.1 FTIR spectroscopy

FTIR spectra were obtained on a Shimadzu spectrophotometer (IRAffinity-1S). Analyses were performed using the KBr pressing method within the spectral range between 4000 and 400 cm^{-1} at 4 cm^{-1} resolution.

Fig. 2 **a** *Oenocarpus bacaba* Mart fruit, **b** *in natura Oenocarpus bacaba* Mart fibers, and (**c**) *Oenocarpus bacaba* Mart fibers after alkaline modification

2.3.2 Surface functional groups

Analyses to quantify organic functional groups present on the surface of OBM were performed by Boehm titration [21], in which 200 mg of this adsorbent were dispersed into 25 mL of $NaHCO_3$ (0.05 mol L^{-1}), Na_2CO_3 (0.05 mol L^{-1}), NaOH (0.02 mol L^{-1}; 0.1 mol L^{-1}), and HCl (0.02 mol L^{-1}) solutions in Erlenmeyer flasks and stirred for 24 h.

In addition to quantifying existing organic functional groups, Boehm titration was employed to better understand the adsorption process. To this end, samples were filtered through filter paper and excess acid and base were determined by titration in triplicate (± 0.1 standard deviation) with NaOH (0.1 mol L^{-1}) and HCl (0.1 mol L^{-1}) solutions, respectively. Surface groups were analyzed as follows: $NaHCO_3$ (carboxylic groups), Na_2CO_3 (carboxylic groups and lactones), NaOH (carboxylic groups, lactones, and phenolic groups), and HCl (basic sites) [22].

2.3.3 Point of zero charge (PZC)

The PZC of the adsorbents was determined by placing 50 mg them in contact with 20.0 mL of aqueous solution of NaCl (0.1 mol L^{-1}) at pH between 2.0 and 12.0 for 24 h. NaOH (0.1 mol L^{-1}) and HCl (0.1 mol L^{-1}) solutions were used to adjust the pH. The supernatant was filtered and the final pH was measured. PZC was determined by calculating the difference between initial and final pH values (i.e., $\Delta pH = pH_f - pH_i$), where ΔpH was plotted against pH_i and the PZC was obtained from the intersection of the lines [18, 23].

2.3.4 Thermogravimetric analysis (TGA)

TGA was carried out in an alumina capsule with approximately 15 mg of material, which was subjected to a heating rate of 10 °C min^{-1} from 0 to 800 °C under nitrogen atmosphere on a TGA-51 Shimatzu instrument at an N_2 flow rate of 20 mL min^{-1}.

2.3.5 Determination of surface area (BET method)

Physical adsorption of nitrogen at low temperatures (− 196.15 °C) was used to measure the surface area by BET (Brunauer–Emmett–Teller method) on an ASAP 2010 Micrometrics instrument and using BJH (Barrett–Joyner–Halenda method) to calculate the pore volume.

2.3.6 Scanning electron microscope (SEM)

Micrographs were obtained by SEM (field emission scanning electron microscopy) on a 7500F JEOL instrument at different magnifications. Samples were covered with a thin layer of gold, using a sputter coater, and analyzed under a scanning electron microscope. A 250 kV electron beam was employed, which enabled the researchers to obtain micrographs of the physical structure of the surfaces of the adsorbents under investigation.

2.3.7 X-ray diffraction

XRD data (X-ray diffraction) were obtained on a D2 phaser diffractometer equipped with a LinxEye detector, operating with CuK α, nickel filter, 30 kV, and 10 mA. Powder diffraction patterns were obtained from 2θ = 8° to 100°, at 0.02 and 5 s/step rate. Peak deconvolution of diffraction patterns was carried out with TOPAS 4.2 software (Bruker-AXS).

2.4 Process evaluation

2.4.1 Effect of initial pH

The effect of pH on adsorption of RhB and MB onto OBMi and OBMm was investigated at different pH values (2.0, 4.0, 6.4, and 10.0), i.e., at pH_{PZC} as well as below and above pH_{PZC}. Initially, pH values of the dye solutions were adjusted using

NaOH and HCl solutions, by adding 200 mg of each adsorbent to 25 mL of 1.1×10^{-5} mol L^{-1} RhB solutions for 60 min. Subsequently, samples were centrifuged at 3500 rpm for 10 min and each dye concentration was calculated from the absorption intensity measured in the supernatant at its maximum absorption wavelength ($\lambda = 554$ nm) on an Agilent UV–Vis spectrophotometer. Removal efficiency was determined according to Eq. (1). This procedure was repeated for MB as contaminant, under the same conditions as those used in the assays with RhB, albeit with initial concentration of 4.1×10^{-5} mol L^{-1} and using the maximum absorption wavelength for MB ($\lambda = 672$ nm).

$$\%R = \frac{(C_i - C_f)}{C_i} x100,$$
(1)

where $\%R$ is removal efficiency and C_i and C_f are initial and final dye concentrations (mol L^{-1}), respectively.

2.4.2 Influence of ionic strength

To investigate the effect of ionic strength on adsorption capacity in the RhB dye solution, concentrations of different electrolytes in the dye solutions (NaCl and CaCl$_2$) ranged from 0.005 to 0.02 mol L^{-1}, at initial concentration of 1.1×10^{-5} mol L^{-1}, pH 4.0 (OBMi), and 6.0 (OBMm), and 25 °C. This procedure was repeated for MB as contaminant under the same conditions as those used in the assays with RhB, albeit with initial concentration of 4.1×10^{-5} mol L^{-1}. Removal efficiency was calculated using Eq. (1).

2.4.3 Biosorbent dose

The effect of OBMi and OBMm dosage on dye removal was tested in the range between 25 and 300 mg, using 25 mL of RhB solution at a concentration of 1.1×10^{-5} mol L^{-1} and pH 4.0 (OBMi) and 6.0 (OBMm). The mixture was stirred for 60 min at room temperature (25 °C). This procedure was repeated using MB as contaminant under the same conditions as those used in the assays with RhB, albeit with initial concentration of 4.1×10^{-5} mol L^{-1}. The removal efficiency was calculated using Eq. (1).

2.5 Adsorption kinetics assays

Kinetics assays were conducted in triplicate (standard deviation ± 0.1), using 25 mL of RhB solution with a concentration of 1.1×10^{-5} mol L^{-1} and 200 mg of OBMm (pH 6.0). The mixture was placed under stirring at 25 °C with 60 min of contact time. The supernatant and dye solution were then reanalyzed for maximum length of dye adsorption. This procedure was repeated using MB as contaminant, under the same conditions used as those used in the assays with RhB, albeit with initial concentration of 4.1×10^{-5} mol L^{-1}. The amount of dye adsorbed as a function of time was calculated using Eq. (2).

$$q_t = \frac{(C_i - C_t) * v * MW}{m},$$
(2)

where q_t (mg g^{-1}) is the amount of RhB/MB adsorbed at time t, C_i (mol L^{-1}) is the initial dye concentration, C_t (mol L^{-1}) is the dye concentration in the aqueous solution at time t, v (L) is the volume of the dye solution used, MW is the molecular weight of each dye (g mol^{-1}) and m (g) is the mass of the biosorbent in question.

2.6 Adsorption isotherms

After the adsorption kinetics assays, isotherm assays were conducted in triplicate (standard deviation ± 0.1) with 25 mL of dye solution and concentration ranging between 10^{-6} and 4.1×10^{-2} mol L^{-1} for MB and between 10^{-7} and 5×10^{-4} mol L^{-1} for RhB, ~ 200 mg OBMm (pH 6.0). The mixture was placed under agitation at controlled temperatures (25 °C and 55 °C) and defined contact time. Then, the dispersion was centrifuged, and the supernatant of each dye solution was analyzed at its corresponding maximum absorption wavelength. The amount of each dye adsorbed as a function of the equilibrium concentration was calculated using Eq. (3).

$$q_e = \frac{(C_i - C_e) * V * MW}{m},$$ (3)

where q_e (mg g^{-1}) is the amount of adsorbed RhB/MB as a function of C_e, and C_e (mol L^{-1}) is the dye equilibrium concentration in the aqueous solution.

2.7 Thermodynamic parameters

The thermodynamic parameters Gibbs free energy (ΔG°), enthalpy (ΔH°), and entropy (ΔS°) were calculated according to Eqs. (4) through (6):

$$K_e = \frac{q_e}{C_e} x \rho,$$ (4)

$$\ln K_e = \frac{\Delta S°}{R} - \frac{\Delta H°}{RT},$$ (5)

$$\Delta G° = \Delta H° - T\Delta S°,$$ (6)

where K_e is the equilibrium constant (dimensionless), ρ is the water density (g L^{-1}), q_e is the amount of dye adsorbent (mg g^{-1}), C_e is the equilibrium concentration of the dye in the solution (mg L^{-1}), R is the universal gas constant (8.314 J mol^{-1} K^{-1}) and T is temperature (K). ΔH° (J mol^{-1}) and ΔS° (J mol^{-1} K^{-1}) can be calculated from the slope (ΔH°/R) and intercept (ΔS°/R) of the plot $\ln K_e$ vs $1/T$.

2.8 Desorption assays

To carry out the batch adsorption process, 25 mL of aqueous dye solution (3.0×10^{-5} mol L^{-1}) were placed in contact with 200 mg of OBMi or OBMm under stirring for 60 min. Post-adsorption samples were collected, dried at 90 °C for 12 h, and placed in contact with 25 mL of ethanol at pH 4.0 (OBMi) and 6.0 (OBMm) under agitation for 10 min. After the adsorbents were separated by centrifugation, the supernatant was analyzed by ultraviolet–visible spectroscopy to estimate the amount of desorbed dye. The adsorption/desorption assays were performed three times, with two recycling cycles. The desorption rate was calculating by Eq. (7) [24].

$$\%D = \frac{C_d}{C_a} x 100,$$ (7)

where *%D* is desorption efficiency, C_a is the concentration of adsorbed dye (mol L^{-1}) and C_d is the concentration of desorbed dye (mol L^{-1}).

3 Results and discussion

3.1 Characterization of biosorbents

3.1.1 FTIR measurements

The presence of surface functional groups observed through Boehm titration was obtained by FT-IR spectroscopy for OBMi and OBMm before adsorption (Fig. S1).

OBMi and OBMm infrared spectra indicate the presence of functional groups typical of lignicellulosic materials before and after biosorption. The stretching band at around 3.425 cm^{-1} obtained for OBMi and OBMm can be attributed to O–H stretching vibrations of hydrogen-bonded hydroxyl groups (from alcoholic, carboxylic or phenolic groups) and water adsorbed on the surface [25]. The bands at 2.920 and from 2.852 to 2.839 cm^{-1} are attributed to C-H bond stretching in methyl and methylene groups [18, 26–29].

The region between 1.750 and 1.600 cm^{-1} is characteristic of lactone, carboxylic, and carbonyl acid groups. The intense band at 1.648 cm^{-1} is characteristic of C=O bonding in carbonyl groups and the band at 1.045 cm^{-1} is related to C–O bonding in esters [29]. According to Takeno et al., the band at 1.453 cm^{-1} is due to CH$_2$ scissoring motion in cellulose and hemicellulose. This band is associated to Type I cellulose crystals, an expected result since most tall plants feature this type of structure. Aromatic C=C stretching vibrations occur between 1.510 and 1.455 cm^{-1}. The vibration peak at 896 cm^{-1} corresponds to C–O–C stretching vibration at β-(1 → 4) glycosidic linkage in cellulose [26].

FTIR spectra for OBMi and OBMm indicate that their outer surface is rich in numerous functional groups containing oxygen from carboxylic and carbonyl species. These active surface groups may be responsible for increasing adsorption of cationic species such as MB and RhB due to electrostatic interactions.

3.1.2 Surface groups

Surface groups evidence the prevalence of acidic sites in OBMi and OBMm, as shown in Table 1.

The larger number of acidic sites indicates that the surface may have OH groups, resulting in greater adsorption capacity of cationic dyes.

3.1.3 Thermogravimetric analysis (TGA)

TGA was performed before and after chemical modification. OBMi and OBMm thermal stability was evaluated at the adsorption temperatures used in this study (Fig. 3).

OBMi and OBMm TGA curves show four distinct stages of weight loss as a function of temperature (Fig. 3). Initially (i.e., from 40 to 100 °C), there is loss of water adsorbed onto the surface of both adsorbents. Only at around 200 °C does degradation of the materials begin. This behavior is indicative of good thermal stability of OBMi and OBMm, suggesting that these biosorbents can be used without affecting adsorption at temperatures above 50 °C.

The second and third stages depict hemicellulose and cellulose degradation [25, 30]. The total mass loss at these stages is approximately 44% for OBMi and 55% for OBMm. The last stage occurred between 380 °C and 800 °C, denoting lignin degradation (≈ 16%). At this stage, it is also possible to observe that chemical modification reduced the amount of lignin in OBMm, which was also reported in other studies [2, 10]. At the end of the analysis, 30.83% and 21.58% of residues (mostly carbonaceous) were obtained with OBMi and OBMm, respectively.

3.1.4 Surface area (BET method)

OBMi and OBMm surface areas are directly related to their adsorption capacity, hence their surface areas as well as their pore volumes were quantified (Table 2).

It should be noted that OBMm pore volume and surface area increased substantially after chemical modification in basic medium when compared to those of OBMi. This effect is probably due to partial lignin degradation (the outermost part of fibers) caused by NaOH [31].

3.1.5 Scanning electron microscope (SEM)

OBMi and OBMm SEM micrographs at × 250, × 500, and × 1000 magnifications are shown in Fig. 4a–f.

Table 1 Surface groups quantified by Boehm titration for OBMi and OBMm	Surface functional group	OBMi (mM g^{-1})	OBMm (mM g^{-1})
	Lactone	2.22	4.45
	Carboxylic acid	2.32	3.46
	Phenolic	0.45	0.97
	Acid groups (total)	4.99	8.88
	Carbonyl	3.63	6.34
	Other base groups	1.03	0.14
	Base groups (total)	4.66	6.48

Fig. 3 TGA curves for OBMi (**A**) and OBMm (**B**) under N_2 atmosphere at 10 °C/min heating rate
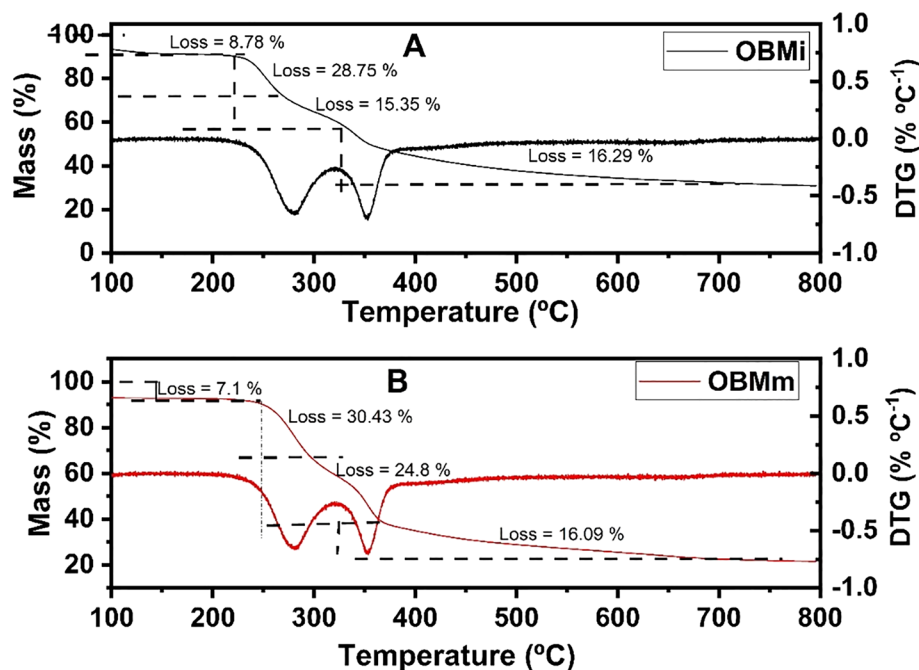
Table 2 Surface area and pore volume for OBMi and OBMm

Biosorbent	Surface area ($m^2\,g^{-1}$)	Pore volume ($cm^3\,g^{-1}$)
OBMi	0.21	0.0006
OBMm	0.53	0.1220

Micrographs of the biosorbent after chemical modification (OBMm) show pores with larger diameter as compared to the ones shown in the images obtained before modification (OBMi). This result corroborates the aforementioned values obtained by means of BET.

3.1.6 X-ray diffraction (XRD)

Figure 5 shows XRD patterns for OBMi and OBMm. The broad diffraction background and the absence of a thin band in both XRD profiles are indicative of predominantly amorphous structures [2, 16]. The characteristic crystalline cellulosic component can be identified by three peaks at 2θ values of ~ 15°, 22°, and 35° (Fig. 5a, b).

The crystalline structure of cellulose is primarily attributed to Van der Waals forces and hydrogen bonding interactions between adjacent molecules. On the other hand, hemicellulose and lignin confer the amorphous characteristic to the material [32, 33]. Lastly, the diffraction profile of native cellulose can be observed, in agreement with FTIR data evidencing a band at ~ 1450 cm^{-1} (typical of Type I cellulose) and with TGA data showing a peak at 320 °C implying cellulose degradation.

3.1.7 Point of zero charge (PZC)

OBMi and OBMm PZCs (Fig. S2) were 3.1 and 7.3, respectively, corroborating the data obtained by means of FTIR and Boehm titration, since the concentration of acid groups in OBMm virtually doubled as compared to that in OBMi, in agreement with the slightly basic pH of OBMm (7.3). At pH values lower than 3.1 (OBMi) and 7.3 (OBMm), the surfaces of the adsorbents are positively charged and, thus, more suitable for adsorbing anionic dyes.
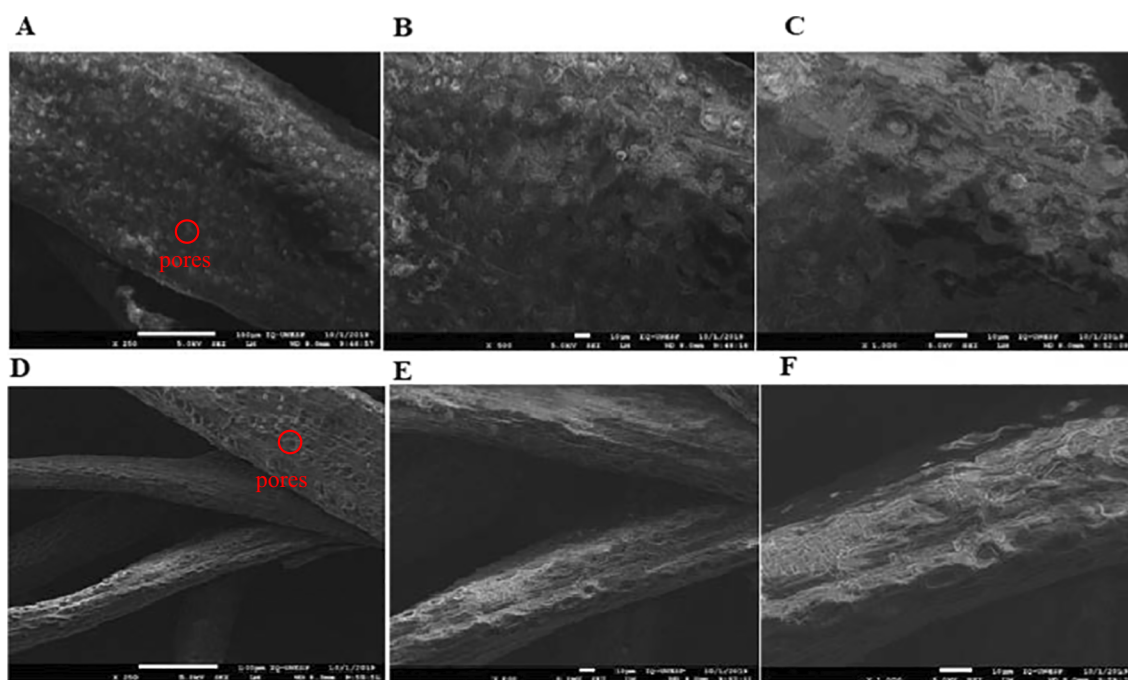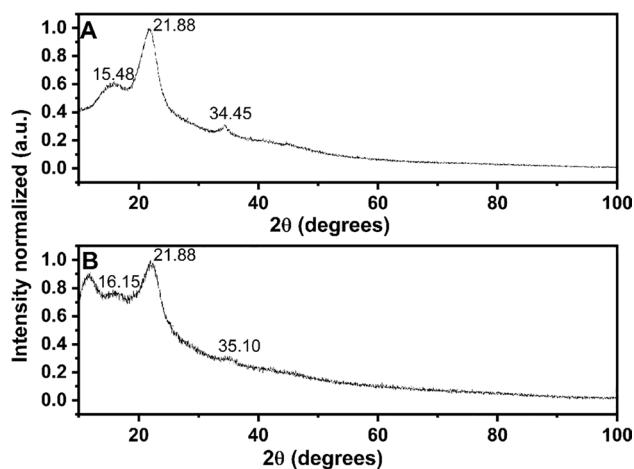
Fig. 4 SEM images of OBMi (**a–c**) and OBMm (**d–f**) samples before adsorption at ×250 (**a/d**), ×500 (**b/e**), and ×1,000 (**c/f**) magnifications, respectively

Fig. 5 XRD patterns for (**A**) OBMi and (**B**) OBMm (dried at 80 °C for 24 h)

3.2 Effect of operating parameters

3.2.1 Effect of initial pH

The effect of initial pH on OBMi and OBMm removal efficiency of RhB and MB dyes is shown in Fig. S3.

At the pH values under investigation, OBMm adsorption efficiency was superior to that of OBMi for both dyes. Removal efficiency was observed to be pH dependent, i.e., removal of contaminants was higher at more basic pH values, most likely due to their cationic nature. Thus, the increased efficiency of OBMm as compared to that of OBMi was caused by an increase in surface area after modification, corroborated by BET and SEM results.

RhB removal efficiency by OBMm at pH 2.0, 4.0, 6.4, and 10.0 was 29.8%, 72.3%, 91.8%, and 90.7%, respectively, and that of MB by OBMm at pH 2.0, 4.0, 6.4, and 10.0 was 29.7%, 74.2%, 96.2%, and 91.0%, respectively. In both systems, i.e., OBMm:RhB and OBMm:MB, removal efficiency values diverged from the trend observed in OBMi. Nevertheless, this

trend may be related to the ionization degree of RhB and MB, since RhB is neutral at pH > 7 but MB is neutral at pH > 5.6. These factors favor electrostatic interactions between RhB/MB and OBMi and between RhB and OBMm whereas chemical modification favors ion–dipole interactions between OBMm and MB as OBMm removal efficiency was significantly higher at pH ≥ 6.4 [11, 34].

3.2.2 Influence of ionic strength

Ionic strength can, to some extent, affect electrostatic interactions between adsorbents and adsorbates, while electrolytes can influence adsorption behavior by competing with adsorbates on the adsorbent surface. The effect of ionic strength on adsorption of MB/RhB molecules onto OBMi/OBMm surfaces is shown in Fig. S4.

Electrostatic interactions between adsorbent surfaces and adsorbed ions were of an attractive nature. Therefore, an increase in ionic strength causes an increase in adsorption capacity. On the other hand, when electrostatic interactions are of a repulsive nature, adsorption capacity increases proportionately to an increase in ionic strength [35]. OBMi adsorption capacity was observed to increase with increasing ionic strength, which points to significant electrostatic interactions, corroborating Al Ashik et al. [8] in whose study RhB ionization occurred at pH 4.

At pH 4 in this study, negatively charged OBMi particles interacted with the positively charged portion of ionized RhB (located at the basic side, i.e., amine). On the other hand, RhB adsorption increased marginally in OBMm, likewise indicating electrostatic interactions. OBMm was positively charged at pH 6.4, pointing to electrostatic interactions with the negative side (located on the acidic side, i.e., carboxylate group).

With regard to MB, OBMi also interacted electrostatically, since at pH 4 MB is positively charged and OBMi is negatively charged, in addition to exhibiting higher adsorption efficiency with increasing ionic strength. In addition, the results suggest ion–dipole interactions between MB and OBMm as the former is in its molecular form at the pH used in the assay (pH = 6.4) and removal efficiency does not increase significantly with increasing ionic strength.

3.2.3 Effect of biosorbent dosage

This study evaluated the influence of adsorbent mass on dye removal (Fig. 6).

When biosorbent dosage increased from 25 to 200 mg so did RhB and MB removal. For instance, the rise in dye removal efficiency from approximately 40% to 95% in OBMm:RhB and from approximately 25% to 80% in OBMm:MB can be attributed to an increase in sorption surface area and absorption sites [36]. On the other hand, when OBMm dosage increased from 200 to 300 mg, removal percentage decreased in both systems, probably due to the fact that as the adsorbent mass increases so does the medium viscosity, hindering RhB and MB diffusion to the biosorbent surface in the medium [37].

Fig. 6 Effect of adsorbent dosage on RhB and MB adsorption onto OBMm
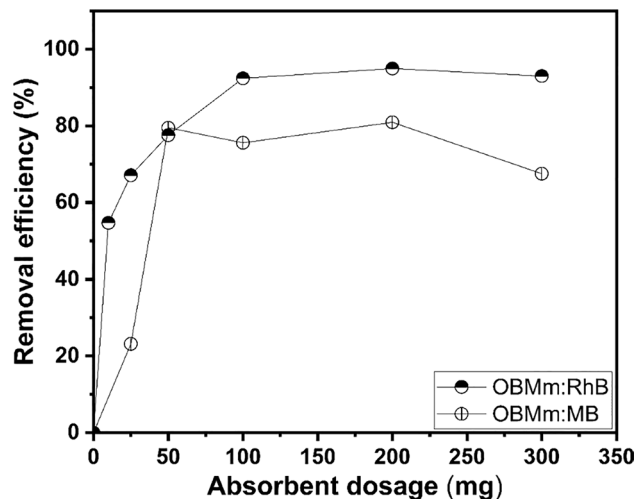
3.2.4 Adsorption kinetics

Figure S5 shows the results obtained from the contact time assays for OBMm:RhB and OBMm:MB up to equilibrium, which occurred after 60 min of contact time.

The amount of adsorbed RhB and MB was directly proportional to contact time. RhB and MB adsorption onto OBMm was initially fast, an indication of this biosorbent having high affinity with the dyes under investigation. Initial affinity is likely related to the large number of vacant surface sites available for adsorption during the initial stage. Near equilibrium, the remaining vacant surface sites were difficult to fill due to slow pore diffusion of solute molecules in the solid and in the bulk phase.

Three kinetic adsorption models were selected to model the adsorption data: pseudo-first-order model (Eq. 8) [7], pseudo-second-order model (Eq. 9) [38], and intraparticle model (Eq. 10) [39], whose equations are described below.

$$q_t = q_e \left(1 - e^{-K_1 t}\right), \tag{8}$$

$$q_t = \frac{K_2 q_e^2 t}{1 + K_2 q_e t}, \tag{9}$$

$$q_t = K_{int} t^{0.5} + C, \tag{10}$$

where q_t and q_e are amounts of RhB and MB adsorbed at time t and at equilibrium (mg g^{-1}), K_1 is the adsorption rate constant of the pseudo-first-order adsorption process (min^{-1}), K_2 is the adsorption rate constant (g mg^{-1} min^{-1}). K_{int} is the intraparticle diffusion rate constant (mg g^{-1} min$^{-0.5}$) and C is the interception (mg g^{-1}). K_{int} can be estimated from the slope of the linear portion of the adsorbed amount curve (mg g^{-1}) in relation to the square root of time (t$^{-0.5}$).

Table 3 shows the kinetic parameters obtained by means of the above mathematical models.

At 2 min of contact time, ~ 30% of RhB was adsorbed, while 60% of MB was adsorbed during the same period. At 10 min of contact time, ~ 70% of both dyes were removed, which is corroborated by data obtained using the aforementioned kinetic models: the rate constant for MB was four times higher than that for RhB.

The theoretical values of maximum adsorption capacity for RhB and MB—where q_e is equal to 1.06 mg g^{-1} and 1.26 mg g^{-1}, respectively, as both fit the pseudo-second order model—were similar to those obtained experimentally, i.e., 1.022 mg g^{-1} and 1.307 mg g^{-1}. This is an indication that the adsorbate-adsorbent interactions were proportionate to two sites for each molecule and involved valence forces in which electron exchange or sharing occurs [33].

The intraparticle diffusion model is related to adsorbate diffusion onto the biosorbent surface. Figure S5 shows the adjusted $Qt \times t^{0.5}$ curve. This figure evidences that the curve does not pass through the origin and features two linear regions, suggesting that intraparticle diffusion is not the step that controls RhB and MB adsorption onto OBMm.

Table 3 Kinetic parameters of RhB and MB adsorption in OBMm (25 mL solution volume; 200 mg adsorbent mass; 25 °C; 9.63 mg L^{-1} dye solution concentration)	Biosorbents	Parameter	Pseudo-first-order model	Pseudo-second-order model	Intra-particle model
	OBMm:MB	Q$_e$ (mg g^{-1})	1.165	1.263	–
		K$_1$ (min^{-1})	0.450	–	–
		K$_2$ (g mg^{-1} min^{-1})	–	0.400	–
		K$_{int}$ (mg g^{-1} min$^{-0.5}$)	–	–	0.125
		C (mg g^{-1})	–	–	0.428
		R^2	0.817	0.906	0.794
	OBMm:RhB	Q$_e$ (mg g^{-1})	0.966	1.064	–
		K$_1$ (min^{-1})	0.109	–	–
		K$_2$ (g mg^{-1} min^{-1})	–	0.145	–
		K$_{int}$ (mg g^{-1} min$^{-0.5}$)	–	–	0.076
		C (mg g^{-1})	–	–	0.328
		R^2	0.952	0.994	0.843

Furthermore, kinetic intraparticle diffusion models resulted in low correlation coefficients, demonstrating that adsorption is not controlled by pore diffusion in OBMm:RhB or OBMm:RhB [39].

3.2.5 Adsorption isotherm

To better investigate the phenomenon of RhB and MB adsorption onto OBMm at different concentrations at 25 °C, both Langmuir (1918) and Freundlich (1907) models of adsorption isotherms were studied. These models are described by Eqs. (11) and (12), respectively.

$$q_e = \frac{Q_m K_L C_e}{1 + Q_m C_e}, \tag{11}$$

$$q_e = K_F C_e^{1/n}, \tag{12}$$

where C_e and q_e are obtained from Eq. (3), Q_m is maximum monolayer absorption onto the adsorbent (mg g^{-1}); K_L (L mg^{-1}) is the Langmuir constant related to adsorption site affinity for MB and RhB; Q_{max}^0 is the theoretical maximum sorption capacity of the adsorbent (mg/g); K_F is the Freundlich equilibrium constant [(mg g^{-1})(mg L^{-1})^n], indicative of absorption capacity; n is the Freundlich constant related to sorption intensity and heterogeneity; and $1/n$ (dimensionless)—a function of the adsorption strength—indicates the type of isotherm.

Langmuir and Freundlich adsorption isotherm curves are shown in Figure S6a, b, respectively, and model fits are summarized in Table 4. The best fit for each isotherm model was assessed in terms of R^2 (distribution coefficient).

The above data indicate that both biosorption systems are well fitted to the Langmuir and Freundlich models. Comparing both models, the correlation coefficient (R^2) of the Langmuir isotherm was 0.999, and RMSE were 0.221 and 2.480 for OBMm:RhB and OBMm:MB, respectively, indicating that the adsorption at equilibrium fit the Langmuir isotherm model better than the Freundlich isotherm model, because Langmuir model showed higher R^2 values and lower RMSE values, thereby suggesting that the dye was adsorbed onto the adsorbent surface in the form of overlaid monolayers [18].

The high value obtained for K_F suggests that OBMm adsorbed the dye solution easily. The n value indicates the degree of non-linearity between the two stages. For $n = 1$, adsorption is linear; if $n < 1$, adsorption is a chemical reaction; and if $n > 1$, adsorption is a physical process [36]. The values of n for OBMm:RhB and OBMm:MB are 1635 and 2260, respectively, demonstrating that adsorption in both cases is a physical process. Also, n is a measure of isotherm deviation from linearity and is a heterogeneity factor. The value n defines isotherms as S-type, L-type, and C-type according to the Giles adsorption isotherm classification: $n < 1$ describes S-type isotherms, $n = 1$ C-type isotherms, and $n > 1$ L-type isotherms [18].

The value of n is greater than 1 for both adsorption systems (Table 2), indicating that it consists of a physical process and an L-type isotherm. Moreover, when the value of $1/n$ is between 0 and 1, the isotherm is favorable; if $1/n = 0$, it is irreversible; and when $1/n > 1$, it is unfavorable. In this study, $1/n$ for OBMm:RhB and OBMm:MB is 0.61 and 0.44, respectively, so both isotherms are favorable.

Table 4 Langmuir and Freundlich isotherm parameters for RhB and MB adsorption onto OBMm (298.15 K; 25 mL solution volume; 200 mg adsorbent mass; 15 min stirring time)

Biosorbents	Parameters	Langmuir Model	Freundlich Model
OBMm:RhB	Q_m (mg g^{-1})	26.60	–
	K_L (L mg^{-1})	0.00746	–
	K_F [(mg g^{-1})(L mg^{-1})^n]	–	0.630
	N	–	1.635
	R^2	0.999	0.997
	RMSE	0.221	0.317
OBMm:MB	Q_m (mg g^{-1})	407.98	–
	K_L (L mg^{-1})	0.00036	–
	K_F [(mg g^{-1})(L mg^{-1})^n]	–	5.086
	N	–	2.260
	R^2	0.999	0.986
	RMSE	2.480	12.986

Table 5 Different maximum adsorption capacities for methylene blue (MB) and rhodamine B (RhB) onto modified *Onecarpus bacaba* Mart fibers (OBMm) and other adsorbents

Dye	Biosorbent	Q_m (mg g^{-1})	References
Methylene blue	OBMm	407.98	This study
	Moringa oleifera seeds	136.99	[41]
	Dragon fruit peels	195.2	[42]
	Grass waste	364.2	[43]
	Banana stems	101.01	[44]
	Ulva lactuca	344.83	[45]
Rhodamine B	OBMm	26.60	This study
	Clitoria fairchildiana	73.84	[18]
	Palm fruit bunch	69.86	[46]
	Rosemary waste	65.78	[47]
	Tea leaves	53.12	[7]

Table 6 Thermodynamic parameters for adsorption of rhodamine B (RhB) and methylene blue (MB) onto modified *Onecarpus bacaba* Mart fibers (OBMm)

Adsorbent	T (°C)	$\Delta G°$ (KJ mol^{-1})	$\Delta H°$ (KJ mol^{-1})	$\Delta S°$ (J K^{-1} mol^{-1})
RhB	25	− 10.71	3.40	47.33
	35	− 11.18		
	45	− 11.66		
	55	− 12.13		
MB	25	− 8.70	47.78	189.44
	35	− 10.59		
	45	− 12.48		
	55	− 14.38		

The maximum adsorption capacity (Qm) for OBMm:RhB and OBMm:MB, as determined by means of the Langmuir model, is 26.60 mg g^{-1} and 407.98 mg g^{-1}, respectively, greater than the capacities found for biosorbents prepared with oil palm fruit (69.86 mg g^{-1}) [40] and black tea leaves (53.12 mg g^{-1}) [7]. These data evidence the remarkable adsorption performance of OBMm, especially in OBMm:MB. Table 5 shows comparative RhB and MB adsorption capacities for OBMm and other adsorbents found in the literature.

3.2.6 Thermodynamic parameters

The Van't Hoff equation can provide data on thermodynamic parameters of the OBMm:RhB and OBMm:MB adsorption processes.

Both processes indicate a rise in adsorption with increasing temperature, implying endothermic processes. Table 6 shows values of $\Delta H°$, $\Delta S°$, and $\Delta G°$, using the data obtained at the last points in Figures S7a-b.

All positive $\Delta H°$ values indicate that RhB adsorption onto OBMm constituted an endothermic process. The negative $\Delta G°$ values point to thermodynamic viability and spontaneity of the adsorption process. $\Delta G°$ decreased with increasing temperature, indicating that adsorption of RhB molecules increases at higher temperatures. Also, it is physical in nature as physisorption $\Delta H°$ lies usually between − 20 and 0 kJ/mol.

Moreover, physisorption and chemisorption can also be classified by the value of enthalpy change, whose binding forces greater than 84 kJ/mol are thought to be related to physisorption binding [48]. Thus, the dominant physisorption mechanism is probably due to Van de Waals forces and electrostatic attractions between oppositely charged RhB:MB molecules and adsorbents [18, 49].

Positive OBMm:MB and OBMm:RhB $\Delta H°$ confirms the endothermic nature of the process. Furthermore, positive $\Delta S°$ values corroborate the increased randomness of the adsorbent-dye interface and indicate affinity between RhB and MB during adsorption. In addition, positive $\Delta S°$ values reveal that the ordering trend decreased in the system after RhB was adsorbed onto OBMm. This may be attributed to cationic interaction between this dye and OBMm, leading to an increase in the degree of freedom of the system [16].

Negative ΔG° value indicates that RhB and MB adsorption processes are spontaneous and favorable [16, 36]. However, the low adsorption capacity found in OBMm:RhB suggests that equilibrium is reached with a very small amount of RhB present on the material surface. The efficiency data corroborate the low ΔG° values shown in Table 3. Additionally, the adsorption process is governed by entropy variation.

3.2.7 Desorption assays

Adsorption and desorption percentages of MB and RhB were investigated to determine the reuse performance of the adsorbents (OBMi and OBMm), as shown in Fig. 7.

Adsorption capacity increases in the four systems from the 1st to the 3rd cycle, within 10 min of contact time. With regard to desorption, a different situation can be observed when comparing the biosorbent before and after modification. For the system using OBMi, %R is close to that of adsorption (Fig. 7a, b), while OBMm causes a decrease in desorption (Fig. 7c, d), which may be due to electrostatic interactions being stronger in OBMi:RhB/MB than in OBMm:RhB/MB.

As a final point, both adsorbents were capable of being used in three cycles maintaining high adsorption capacity at a consistent MB adsorption/desorption rate, i.e., between 96 and 84%. These data demonstrate that the dyes used in this study—especially OBMm, given that its maximum adsorption capacity was greater than that of OBMi—can be employed to treat water as it can be efficiently recycled without significantly losing its adsorption capacity. This behavior has also been reported for other adsorption systems [49, 50].
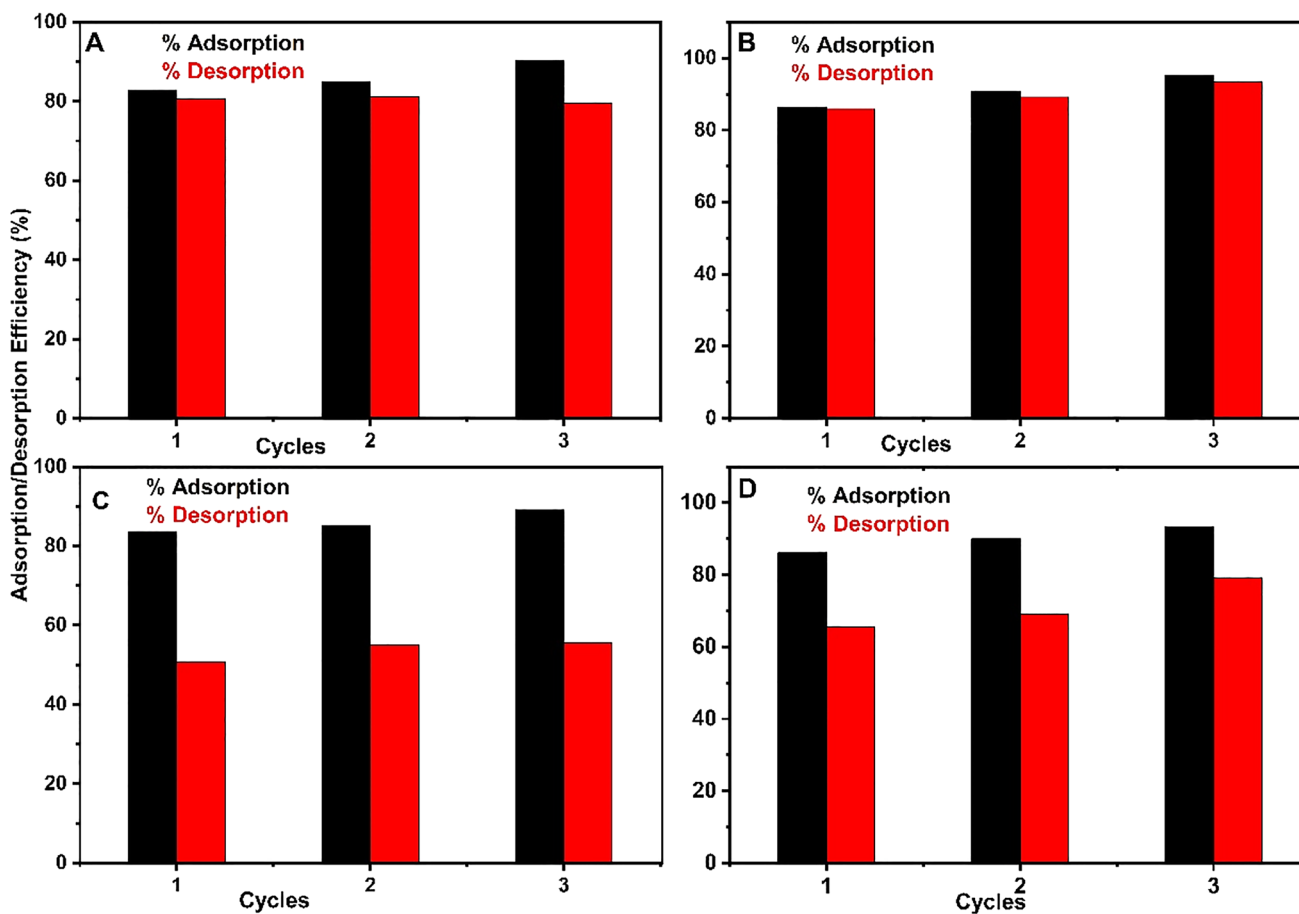
Fig. 7 Removal percentages of reuse cycles (adsorption/desorption) of MB and RhB after adsorption onto OBMi and OBMm in ethanol. **A** OBMi:MB; **B** OBMi:RhB; **C** OBMm:MB; and **D** OBMm:RhB

4 Conclusions

The results obtained in this study show that *Onecarpus bacaba* Mart can be employed as a low-cost adsorbent for removing methylene blue and rhodamine B from water as it displayed good adsorption capacity when compared to other biosorbents. *In natura Onecarpus bacaba* Mart (OBMi) and NaOH-modified *Onecarpus bacaba* Mart (OBMm) exhibited neutral surface charge (PZC) at pH 4.0 and 6.4, respectively. Maximum MB adsorption onto OBMm was 407.98 mg g^{-1} at 25 °C. RhB and MB adsorption processes displayed good fit to the Langmuir isotherm model at 25 °C, indicating pseudo-second-order adsorption kinetics. Thermodynamic assays in this study suggest spontaneous adsorption ($\Delta G° < 0$) and endothermic ($\Delta H° {}^> 0$) processes. Based on the above, it is possible to propose the use of *Onecarpus bacaba* Mart fiber residues for adsorbing different dyes in water treatment.

Availability of data and materials The authors declare that the data supporting the findings of this study are available within the paper and its Additional files. Should any raw data files be needed in another format they are available from the corresponding author upon reasonable request.

Declarations

Ethics approval and consent to participate Registration in the National System for the Management of Genetic Heritage and Associated Traditional Knowledge—SisGen number A1E2414.

Consent for publication Not applicable.

Competing interests The authors have no financial or proprietary interests in any material discussed in this article.

References

1. Peternela J, Silva MF, Vieira MF, Bergamasco R, Vieira AMS. Synthesis and impregnation of copper oxide nanoparticles on activated carbon through green synthesis for water pollutant removal. Mater Res. 2018;21(1).
2. Tabassum M, Bardhan M, Novera TM, Islam MA, Hadi Jawad A, Islam MA. NaOH-activated betel nut husk hydrochar for efficient adsorption of methylene blue dye. Water Air Soil Pollut. 2020;231(8).
3. Bose S, Senthil Kumar P, Rangasamy G, Prasannamedha G, Kanmani S. A review on the applicability of adsorption techniques for remediation of recalcitrant pesticides. Chemosphere. 2023;313.
4. Calicioglu Ö, Bogdanski A. Linking the bioeconomy to the 2030 sustainable development agenda: can SDG indicators be used to monitor progress towards a sustainable bioeconomy? N Biotechnol. 2021;61:40–9.
5. Scrucca F, Ingrao C, Barberio G, Matarazzo A, Lagioia G. On the role of sustainable buildings in achieving the 2030 UN sustainable development goals. Environ Impact Assess Rev. 2023;100:107069.

Discover

6.   Lellis B, Fávaro-Polonio CZ, Pamphile JA, Polonio JC. Effects of textile dyes on health and the environment and bioremediation potential of living organisms. Biotechnol Res Innov. 2019;3(2):275–90.

7.   Hossain MA, Alam MS. Adsorption kinetics of Rhodamine-B on used black tea leaves. Iranian J Environ Health Sci Eng. 2012;9(2):1–7.

8.   Al Ashik A, Rahman MA, Halder D, Hossain MM. Removal of methylene blue from aqueous solution by coconut coir dust as a low-cost adsorbent. Appl Water Sci. 2023;13(3):81.

9.   Naboulsi A, Naboulsi I, Regti A, El Himri M, El Haddad M. The valorization of rosemary waste as a new biosorbent to eliminate the rhodamine B dye. Microchem J. 2023;191:108790.

10. Zhang S, Wang Z, Zhang Y, Pan H, Tao L. Adsorption of methylene blue on organosolv lignin from rice straw. Proc Environ Sci. 2016;31:3–11.

11. Birniwa AH, Mahmud HNME, Abdullahi SS, Habibu S, Jagaba AH, Ibrahim MNM, et al. Adsorption behavior of methylene blue cationic dye in aqueous solution using polypyrrole-polyethylenimine nano-adsorbent. Polymers (Basel). 2022;14(16):3362.

12. Rashid R, Shafiq I, Akhter P, Iqbal MJ, Hussain M. A state-of-the-art review on wastewater treatment techniques: the effectiveness of adsorption method. Environ Sci Pollut Res. 2021;28:9050–66. https://doi.org/10.1007/s11356-021-12395-x.

13. Husien S, El-taweel RM, Salim AI, Fahim IS, Said LA, Radwan AG. Review of activated carbon adsorbent material for textile dyes removal: preparation, and modelling. Curr Res Green Sustain Chem. 2022;5:100325.

14. Şenol ZM, Messaoudi N El, Fernine Y, Keskin ZS. Bioremoval of rhodamine B dye from aqueous solution by using agricultural solid waste (almond shell): experimental and DFT modeling studies. Biomass Convers Biorefin. 2023.

15. Ouardi Y El, Aissouq A El, Chennah A, Ouammou A, Laatikainen K. Synthesis, characterization, and DFT investigation of rhodamine B dye removal by activated carbon produced from argan nutshell. Biomass Convers Biorefin. 2022.

16. Jawad AH, Rashid RA, Ishak MAM, Ismail K. Adsorptive removal of methylene blue by chemically treated cellulosic waste banana (Musa sapientum) peels. J Taibah Univ Sci. 2018;12(6):809–19.

17. Çelik MS, Çetinus ŞA, Yenidünya AF, Çetinkaya S, Tüzün B. Biosorption of Rhodamine B dye from aqueous solution by *Rhus coriaria* L. plant: equilibrium, kinetic, thermodynamic and DFT calculations. J Mol Struct. 2023;1272:134158.

18. da Silva AMB, Serrão NO, de Gusmão CG, Takeno ML, Antunes NTB, Iglauer S, et al. Removal of rhodamine 6G from synthetic effluents using Clitoria fairchildiana pods as low-cost biosorbent. Environ Sci Pollut Res. 2020;27(3):2868.

19. Queiroz MSM, Bianco R. Morfologia e desenvolvimento germinativo de Oenocarpus bacaba MART. (Arecaceae) da Amazônia Ocidental. Rev Árvore. 2009;33(6):1037–42.

20. Valor Econômico Atual ou Potencial de. Plantas Para o Futuro-região norte Oenocarpus spp Bacaba. In: Espécies Nativas da Flora Brasileira de Valor Econômico Atual ou Potencial: Plantas Para o Futuro: Região Norte. 2020. p. 394–412.

21. Oliveira LS, Franca AS, Alves TM, Rocha SDF. Evaluation of untreated coffee husks as potential biosorbents for treatment of dye contaminated waters. J Hazard Mater. 2008;155(3):507–12.

22. Sampaio CG, Freitas FA, Souza FTC, Brito ES, Becker H, Trevisan MTS. Characterization and use of noni (Morinda citrifolia L.) seeds for the removal of hexavalent chromium ions from aqueous solutions. Int J Civil Environ Eng. 2015;15(02):21–31.

23. Celestino GG, Henriques RR, Shiguihara AL, Constantino VRL, de Siqueira MR, Amim JJ. Adsorption of gallic acid on nanoclay modified with poly(diallyldimethylammonium chloride). Environ Sci Pollut Res. 2019;26(28):28444–54.

24. Lee S, Ahn S, Lee H, Kim J. Layer-by-layer coating of MIL-100(Fe) on a cotton fabric for purification of water-soluble dyes by the combined effect of adsorption and photocatalytic degradation. RSC Adv. 2022;12(27):17505–13.

25. Mendonça IM, Machado FL, Silva CC, Duvoisin Junior S, Takeno ML, de Sousa Maia PJ, et al. Application of calcined waste cupuaçu (*Theobroma grandiflorum*) seeds as a low-cost solid catalyst in soybean oil ethanolysis: Statistical optimization. Energy Convers Manag. 2019;200:112095.

26. Maia PJS, Barbosa EM, Vega ML, da Cunha HN, de Souza EA, de Freitas FA. Synthesis and characterization of a perylene derivative and its application as catalyst for ethanol electro-oxidation. Chem Pap. 2018;72(4):1021–30.

27. Maia PJS, Cruz JF, de Freitas FA, de Fátima Freire dos Santos S, de Souza EA. Photophysical properties of a perylene derivative for use as catalyst in ethanol eletrooxidation. Res Chem Intermed. 2019;45(11):5451.

28. Corrêa Santos D, José Sousa Maia P, Antonio de Abreu Lopes M Jr, Sebastián Bello Forero J, Luzia Ferreira de Souza A. A simple isoniazid-based *N*-acylhydrazone derivative as potential fluorogenic probe for Zn^{2+} ions. J Fluoresc. 2021;31:175–84. https://doi.org/10.1007/s10895-020-02651-7.

29. De Souza ALF, Santos DC, Henriques RR, Lopes MAA, Maia PJS, Da Silva AMB, et al. Microwave-assisted synthesis, spectral characterization and DFT studies of Zn(II) complexes based on *N*-acylhydrazone ligands: stability and antioxidant activity. Mediterr J Chemy. 2023;2023(1):64–77.

30. Maia TC, Santaella ST, Maia PJS, de Freitas FA, Oliveira AHB, Costa GB, et al. An integrated assessment to reconstruct the history of changes influenced by multiple anthropogenic activities (City of Fortaleza, Ceará, Brazil). Environ Monit Assess. 2022;194(8).

31. Tan L, Tang YQ, Nishimura H, Takei S, Morimura S, Kida K. Efficient production of bioethanol from corn stover by pretreatment with a combination of sulfuric acid and sodium hydroxide. Prep Biochem Biotechnol. 2013;43(7):682–95.

32. Tran HN, Chao HP, You SJ. Activated carbons from golden shower upon different chemical activation methods: synthesis and characterizations. Adsorpt Sci Technol. 2018;36(1–2):95–113.

33. Tomul F, Arslan Y, Başoğlu FT, Babuçcuoğlu Y, Tran HN. Efficient removal of anti-inflammatory from solution by Fe-containing activated carbon: adsorption kinetics, isotherms, and thermodynamics. J Environ Manage. 2019;238:296–306.

34. Boumediene M, Benaïssa H, George B, Molina St, Merlin A. Effects of pH and ionic strength on methylene blue removal from synthetic aqueous solutions by sorption onto orange peel and desorption study. J Mater Environ Sci. 2018;9(6):1700–11.

35. Al-Degs YS, El-Barghouthi MI, El-Sheikh AH, Walker GM. Effect of solution pH, ionic strength, and temperature on adsorption behavior of reactive dyes on activated carbon. Dye Pigment. 2008;77(1):16–23.

36. Murthy HCA, Desalegn T, Kassa M, Abebe B, Assefa T. Synthesis of green copper nanoparticles using medicinal plant Hagenia abyssinica (Brace) JF. Gmel. leaf extract: antimicrobial properties. J Nanomater. 2020;2020.

37. Bortoluz J, Ferrarini F, Bonetto LR, Crespo JS, Giovanela M. Use of low-cost natural waste from the furniture industry for the removal of methylene blue by adsorption: isotherms, kinetics and thermodynamics. Cellulose. 2020;27:6445–66.

38. Magriotis ZM, Vieira SS, Saczk AA, Santos NAV, Stradiotto NR. Removal of dyes by lignocellulose adsorbents originating from biodiesel production. J Environ Chem Eng. 2014;2(4):2199–210.

39. Simonin JP, Bouté J. Intraparticle diffusion-adsorption model to describe liquid/solid adsorption kinetics. Rev Mex Ing Quim. 2016;15(1):161–73.

40. Teow YH, Tajudin SA, Ho KC, Mohammad AW. Synthesis and characterization of graphene shell composite from oil palm frond juice for the treatment of dye-containing wastewater. J Water Process Eng. 2020;35:101185.

41. Do TH, Nguyen VT, Dung NQ, Chu MN, Van Kiet D, Ngan TTK, et al. Study on methylene blue adsorption of activated carbon made from *Moringa oleifera* leaf. Mater Today Proc. 2020;38:3405–13.

42. Ahmad MA, Eusoff MA, Adegoke KA, Bello OS. Sequestration of methylene blue dye from aqueous solution using microwave assisted dragon fruit peel as adsorbent. Environ Technol Innov. 2021;24:101917.

43. Abdulhameed AS, Firdaus Hum NNM, Rangabhashiyam S, Jawad AH, Wilson LD, Yaseen ZM, et al. Statistical modeling and mechanistic pathway for methylene blue dye removal by high surface area and mesoporous grass-based activated carbon using K_2CO_3 activator. J Environ Chem Eng. 2021;9(4):105530.

44. Misran E, Bani O, Situmeang EM, Purba AS. Banana stem based activated carbon as a low-cost adsorbent for methylene blue removal: isotherm, kinetics, and reusability. Alex Eng J. 2022;61(3):1946–55.

45. Razali NS, Abdulhameed AS, Jawad AH, Athman ZA, Yousef TA, Al-Duaij OK, et al. High-surface-area-activated carbon derived from mango peels and seeds wastes via microwave-induced $ZnCl_2$ activation for adsorption of methylene blue dye molecules: statistical optimization and mechanism. Molecules. 2022;27(20):6947.

46. Manase A. Fixed bed adsorption studies of rhodamine B dye using oil palm empty fruits bunch activated carbon. J Eng Stud Res. 2012;3:3–6.

47. Naboulsi A, Naboulsi I, Regti A, El Himri M, El Haddad M. The valorization of rosemary waste as a new biosorbent to eliminate the rhodamine B dye. Microchem J. 2023;191:108790.

48. Kuo CY, Wu CH, Wu JY. Adsorption of direct dyes from aqueous solutions by carbon nanotubes: determination of equilibrium, kinetics and thermodynamics parameters. J Colloid Interface Sci. 2008;327(2):308–15.

49. Alvarez-Torrellas S, Boutahala M, Boukhalfa N, Munoz M. Effective adsorption of methylene blue dye onto magnetic nanocomposites. Modeling and reuse studies. Appl Sci (Switzerland). 2019;9(21):4563.

50. Elkholy AS, Yahia MS, Elnwawy MA, Gomaa HA, Elzaref AS. Synthesis of activated carbon composited with Egyptian black sand for enhanced adsorption performance toward methylene blue dye. Sci Rep. 2023;13(1):4209.